Advanced Nanoscale Composites

Elena V. Markovic, Alexander K. Rostov, Sophia N. Ilyushina
Institute of Materials Science, Moscow, Russia

***Abstract*—**We report herein the development and preliminary mechanical characterization of fully-dense multi-wall carbon nanotube (MWCNT)-reinforced ceramics and glasses based on a completely new methodology termed High Shear Compaction (HSC). The tubes are introduced and bound to the matrix grains by aid of polymeric binders to form flexible green bodies which are sintered and densified by spark plasma sintering to unprecedentedly high densities of 100% of the pure-matrix value. The strategy was validated across a PyrexTM glass / MWCNT composite while no identifiable factors limit application to other types of matrices. Non-destructive evaluation, based on ultrasonics, of the dynamic mechanical properties of the materials including elastic, shear and bulk modulus as well as Poisson's ratio showed optimum property improvement at 0.5 %wt tube loading while evidence of nanoscale specific energy dissipative characteristics acting complementary to nanotube bridging and pull-out indicate a high potential in a wide range of reinforcing and multifunctional applications.

***Keywords*—**Carbon nanotubes, ceramic matrix composites, toughening, ultrasonics.

I. Introduction

TODAY, scientific effort focuses on the development of a new generation of materials reinforced at a scale three orders of magnitude closer to molecular dimensions than conventional reinforcements by exploitation of carbon nanotubes' (CNT) [1] remarkable combination combination of mechanical [2], [3], transport [4]-[6], optical and electronic properties [7]-[9]. While remarkable progress has been achieved in reinforcing polymers with CNTs [10]-[12], this is not the case for ceramics. Property improvement and toughening of the stiff and brittle ceramic monoliths by CNTs depends critically upon four major factors: a) high tube quality with low impurity content, few structural defects, high crystallinity and high aspect ratios, b) establishment of a homogeneous dispersion of nanotubes within the ceramic and hampering of CNTs' natural tendency to agglomerate/ entangle with extremely undesirable side-effects on material performance, c) achievement of appropriate interfacial bonding between the inorganic matrix and the nano reinforcements to promote toughening through development of energy dissipation mechanisms and d) achievement of high densification levels during the final sintering stage [13]-[15]. All these factors are affected by the ceramic manufacturing and processing routes which involve dispersion of tubes within the inorganic continuous phase and sintering at oxidative environments.

Tube dispersion techniques currently include conventional powder processing [16], in-situ growth in glasses and ceramics [17], colloidal processing [18] and sol-gel processing [19] while sintering is achieved either through hot pressing (HP) [20], hot-isostatic pressing (HIP), pressure-less sintering (PS) [21] and spark plasma sintering (SPS) [22]. Due to limitations specific to the techniques, achievement of fully dense nanotube-reinforced ceramics, where density is -ideally- identical to that of the pure ceramic, is still an open challenge today. For example, the most impressive concept of in situ growth of CNTs in ceramics provides materials with remarkable inherent CNT homogeneity that may, nonetheless, suffer from incomplete sinterability due to CNTs pinned at grain boundaries blocking densification [19]. On the other hand, PS suffers from the requirement of extremely hostile for the nanotubes- temperatures, above 1300oC, to yield fully dense ceramics [20]. In H(I)P and PS, heat provided externally to the sample is frequently associated with non-uniform sintering pattern throughout material volume. Among different sintering methods, SPS stands out as it is associated with higher final densities, lower sintering temperatures and shorter processing durations, leading to ceramics of superior properties [16], [23]-[25]. In one notable case, a fully dense nanotube-alumina ceramic with unprecedented toughening characteristics was recently processed via SPS by [26]. Lowering of production costs and upscaling of production rates of CNT-ceramics that will unfold their application potential are also issues that remain to be resolved.

Here, we propose a completely new, highly scalable, low cost methodology for large scale production of 100% dense carbon nanotube-reinforced ceramics starting from flexible green (unfired) sheets of ceramic powder and homogeneously embedded nanotubes bound by High Shear Compaction (HSC). HSC is a state of the art, continuous production tape forming process, wherein powders are closely packed by water-based binders subject to high shear forces while the material is maintained at a very high viscosity. HSC is superior to other tape forming processes including tape casting, roll compaction, slip casting and powder pressing in that i) it allows density prediction by control of degree of compaction, ii) particles cannot settle hence non-uniform particle size distribution typical with casting technologies is prevented, iii) particles sheared against one another close-pack to green densities higher than any other tape forming process, a feature which tremendously aids sinter ability, iv) resultant sheets are completely isotropic with greatly

reduced fired shrinkage variation while, v) they are flexible enough to be easily post-formed into complex shapes.

Green CNT-glass sheets of record-breaking surface areas of 0.5 m^2 were manufactured during this study while the process is scalable to 350 m^2 sheets of widths up to 8 m at a production rate of 1.5 m per minute. The green product is flexible enough to allow forming into virtually any geometry and stacking for the production of an unlimited range of three-dimensional structures. Green CNT-ceramic disks of varying nanotube loadings underwent a single-step SPS cycle for binder burnout and sintering during which unconventional densification levels, to 100% of the pure ceramic, were achieved. A borosilicate Pyrex glass was utilized as continuous phase and long multi-walled CNTs as reinforcement while no apparent factors limit the application of the technique to other phases or hybrid materials. The material exhibited significant stiffness improvement under both shear and axial elastic loads while indications of nanoscale and micro-scale toughening mechanisms endow great application potential.

II. EXPERIMENTAL

Pyrex borosilicate glass, Corning code 7740, a low expansion glass resistant to chemical attack and conforming to ASTM E-438, was provided in powder form by Corning Refractories (Corning, NY, USA). The nominal density, Young's modulus, shear modulus and Poisson's ratio of the glass were quoted as 2.23 g/cm^3, 64 GPa, 26.7 GPa and 0.2, respectively. Multi-wall carbon nanotubes (MWCNT) of nominal purity higher than 97% and amorphous carbon content of less than 3%, synthesized via catalytic chemical vapor deposition were acquired by Shenzhen Nanotech Port Co. Ltd (Shenzhen, China). Nominal tube diameter ranged from 20 to 40nm while their length ranged from 5 to 15μm.

Our strategy for fabrication of fully dense MWCNT/Pyrex borosilicate glass is summarized in Fig. 1. Therein, surfactant assisted aqueous suspensions of the tubes were initially prepared by addition of sodium dodecyl sulphate (SDS, Sigma-Aldrich code 436143, Sigma-Aldrich Chemie Gmbh, Munich, Germany) and of MWCNTs, at an 1/1 weight ratio, in 1500 cm^3 (1.5 liter) triple-distilled water in standard Pyrex glass beakers and subsequent ultrasonic processing at a frequency of 24kHz, for 20 minutes. A Ø22mm cylindrical nontrade operating on a Hielscher UP400S device (Hielscher Ultrasonics GmbH, Teltow, Germany) was used to deliver a power throughput of 4500 J/min to the tubes. The specific combination of ultrasonic energy and processing duration was established as optimum for achievement of homogeneous dispersions of the tubes in the target volume without significant degradation of their initial length. The latter task involved a tedious parametric analysis of CNT agglomerate size variation with ultrasonication time and energy, by dynamic light scattering and laser diffraction.

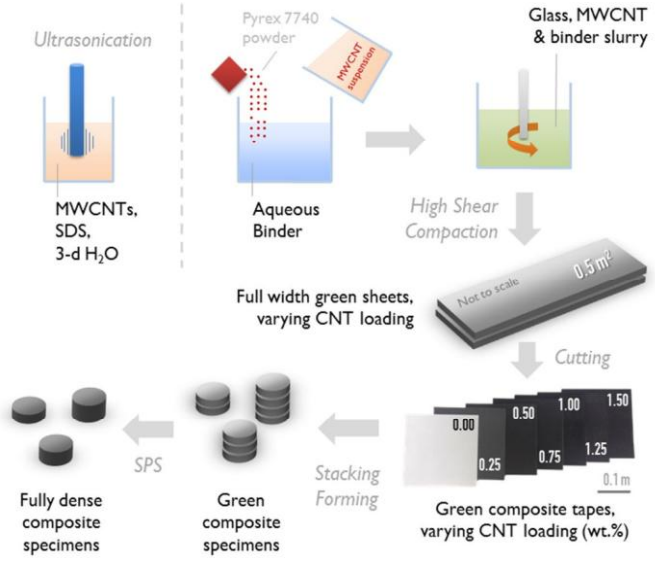

Fig. 1 Graphical overview of proposed route for fabrication of MWCNT ceramics

Using the nominal borosilicate glass density value of 2.23 g/cm^3, appropriate amounts of aqueous MWCNT suspensions were calculated and added to the HSC binder to yield sheets of variable CNT loadings within 0 to 1.5% wt., step of 0.25% wt. The resultant MWCNT/borosilicate glass green sheets had record-breaking surface areas of 0.5 m^2 per formulation, thickness of 3mm and were cut into 125 x 125 mm^2 green plates.

Sets of four 20mm diameter disks were cut from green plates of each MWCNT formulation; the disks were stacked and sintered in a SPS HPD 25/1 machine (Fine Ceramics Technologies GmbH, Germany) equipped with a graphite die of an internal diameter of 20 mm. All experiments were performed under vacuum of 8.10-2 mbar, a standard feature of the technique which was nonetheless indispensable for preventing carbon nanotube oxidation/loss during residence of the material of the present study at the high temperatures required for sintering of the borosilicate glass. A punch pressure was applied to all samples before heating and was retained through the entire thermal cycle duration; pressure was progressively removed during cooling. A pulse sequence consisting of 10ms of pulse current followed by 5ms of current without pulse was chosen. To identify the optimal sintering temperature for achievement of fully dense samples, the real-time densification rate of the ceramic, quantified by means of displacement speed of the mobile upper punch of the apparatus, was investigated. Bulk densities of samples were measured through Archimedes' method following standard test method ASTM C373-88. The thermal cycle used for all specimens consisted of 4 stages: initial heating to 200°C with a rate of 100°C/min; followed by heating to 300°C at a rate of 10°C/min; then heating to 500°C at a rate of 5°C/min and the final heating stage consisted of heating to the target sintering temperature (600, 650, or 700°C) at a rate of 15°C/min. Samples were not allowed soaking time at the sintering temperature; a natural cooling step, duration of ca. 10 min, completed the thermal cycle. The total duration of the thermal cycles was ca. 90 min. Four-layer CNT-ceramic samples

had a thickness of 4.5±0.1 mm after SPS; the associated degree of compaction from their initial green condition was calculated as 68%.

The four elastic constants of the sintered compacts, namely, Young's modulus, shear modulus, bulk modulus and Poisson's ratio were measured non-destructively at zero-load by the ultrasonic methodology previously described in [27]. In brief, the velocities of propagation of ultrasonic waves -which are elastic stresses of small amplitude- are directly related to the elastic moduli of the material at zero-load (dynamic moduli). Knowledge of shear and longitudinal velocities, makes feasible the computation of all four elastic constants through (7)-(10) in [27]. In the current study, ultrasonic wave velocities were measured using piezoelectric transducers with x-cut or y-cut crystals, for longitudinal and shear wave generation, respectively, operating in pulse-echo mode. The ultrasonic frequencies of 15 and 5MHz were used for longitudinal and shear waves, respectively, so that the wavelength of ultrasound was much smaller than specimen thickness. The microstructure of polished surfaces of fully dense CNT-ceramic specimens was examined in a Zeiss SUPRA 35VP scanning electron microscope equipped with a 30 kV electron beam.

III. Results and Discussion

Given the detrimental effect of incomplete densification on ceramic materials' performance, tuning of sintering parameters for the achievement of fully dense samples was a key concern in the present study. In terms of punch pressure, typical values of 16 and 32 MPa were tested and the latter was found associated with higher densification levels. Higher values were not tested as potentially harmful to material integrity. Optimal sintering temperature was established by examination of the real-time densification curves of the ceramics as shown Fig. 2. It was observed that densification began at ca. 500°C, was maximum at ca. 570°C (nominal annealing temperature for Pyrex 7740 is 560°C) and complete at ca. 630°C. CNT-ceramics sintered at 650°C were found to be fully dense. A much narrower peak, appearing at ca. 330°C in the densification curves was associated with binder burnout, i.e. the very fast decomposition of the material holding the glass grains and tubes tightly bound.

To demonstrate the actual effect of sintering temperature on densification, hence also material performance, three final sintering temperatures of 600, 650 and 700°C were investigated; the resulting levels of densification, are plotted as a function of tube loading for all seven MWCNT formulations (0-1.5 %wt., step of 0.25 %wt.) in Fig. 3. Sintering at 600°C yielded only partially densified samples with property values appearing systematically lower than both the fully dense case and their 650 and 700°C counterparts. Samples sintered at 650°C were found to be fully dense within the entire nanotube loading range up to 1.25%; density dropped by 0.9% in the ceramic with the maximum MWCNT content, 1.5% wt. A sintering temperature of 700°C appeared to offer similar densification efficiency, however the surprising low densities returned for the pure-borosilicate sample and for the 1.5 %wt. loaded samples did not favor usage of this temperature.

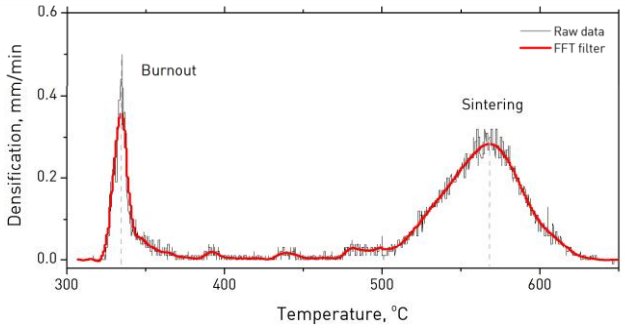

Fig. 2 Real-time densification rate of MWCNT/borosilicate glass as function of temperature during SPS cycle

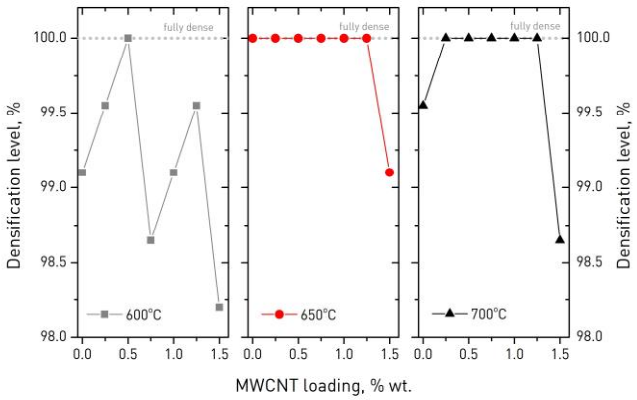

Fig. 3 Degree of densification for MWCNT/borosilicate glass materials with varying tube concentrations as a function of sintering temperature. The y-axis values are obtained by normalization of CNT/ceramic densities measured via the Archimedes method, to the property value achieved for pure borosilicate glass samples.

Contrary to conventional sintering techniques, which involve successive thermal cycles for binder burn-out, sintering and densification, the single-step SPS cycle proposed in the current work is highly efficient, fully customizable and time saving.

The variation of dynamic moduli of MWCNT/borosilicate glass sintered at 600, 650 and 700°C is plotted in Figs. 4 (a) and (b) as a function of sintering temperature and nanotube concentration in the compacts. For samples sintered at 600°C (data represented in red solid square symbols) both property values appeared lower than their nominal pure Pyrex 7740 glass counterparts; this behavior is believed to be directly associated with the low densities of the samples stemming from incomplete sintering at 600°C. Nonetheless, a prominent increase in both moduli appears to occur at 0.5% wt. MWCNT loading, followed by a steep property degradation thereafter. Similar enhancements, in both moduli, for 0.5 % wt. tube loading were noted for the fully dense ceramics sintered at 650ºC, as Figs. 4 (a) and (b) suggest (red solid cycle symbols). For these samples, the values of Young's and shear modulus at 0% loading, 62.5 and 25.9 GPa respectively, compared favorably to the nominal values reported by the glass manufacturer, 64 and 26.7 GPa respectively. Corresponding peak property values at 0.5% wt. loading were 65.7 and 28.5 GPa respectively, increased by 5% and 10% respectively, from their pure-glass counterparts. Both property values appeared to drop to the previous levels as tube

concentrations increased above 0.5 %wt. Moduli enhancements were less prominent in MWCNT/borosilicate glass ceramics sintered at 700°C, where a 5.4% increase was noted in shear modulus at 0.5% wt. loading and a 4.3% increase in Young's modulus was found shifted to 0.75% wt. loading. The observed tendency, of property enhancements being limited at low nanotube loading fractions and further increases in concentration leading to opposite effects, is not an unknown phenomenon for CNT-reinforced ceramics and it is attributed to CNT dispersion deficiency due to agglomeration in high tube loadings [14], [15]. In this context, the very steep drop in moduli observed for samples sintered at 600°C can be rationalized upon the combined effect of incomplete sintering and agglomeration.

The variation of Poisson's ratio and bulk modulus is plotted in Fig. 4 (c) as a function of nanotube loading, for the CNT/ceramic fully densified at 650°C. Both properties are observed to reach minima at the tube concentration previously found associated with the maximum improvement in moduli, i.e. 0.5 % wt. This seemingly unconventional behavior, signifies that both the ceramic's resistance to uniform pressure and the ratio of transverse to axial deformation are least when material resistances to axial and shearing stresses are greatest. In fact, such a condition is not incompatible with theory of elasticity expectations. Therein, Young's modulus, E, is related to bulk modulus, K, and Poisson's ratio, ν, through:

$$E = 3K(1-2\nu) \tag{1}$$

In (1) when ν is minimum, the negative term 2ν can maximize enough to dominate over K minimization, so that the product on the right-hand side of (1), i.e. the material's resistances to axial stress can indeed maximize. Likewise, shear modulus, G, is related to K and ν through

$$G = \frac{3K(1-2\nu)}{2(1+\nu)} \tag{2}$$

Here, minimization of ν leads to the simultaneously maximization of both (1-2ν) and reciprocal 2(1+ν), hence the fraction on the right-hand side of (2), i.e. the material's resistances to shear stress, maximizes more rapidly than in the previous case. This may also explain the higher improvement (10%) for the shear modulus at 0.5% wt. loading, compared to elastic modulus (5%), for CTN/ceramics sintered at 650ºC.

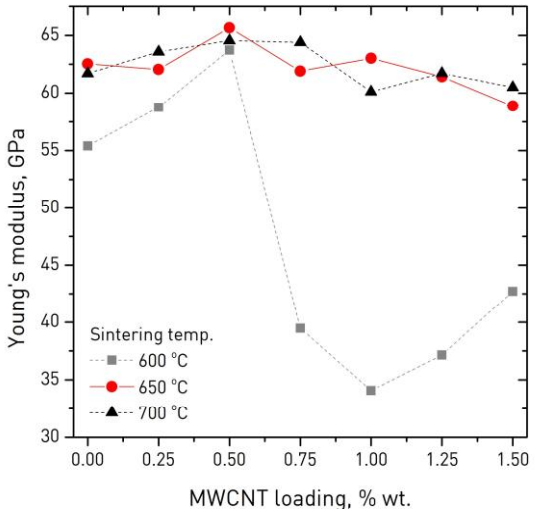

(a)

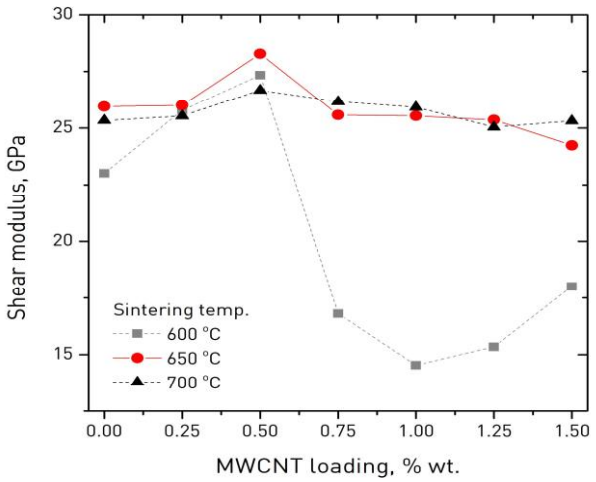

(b)

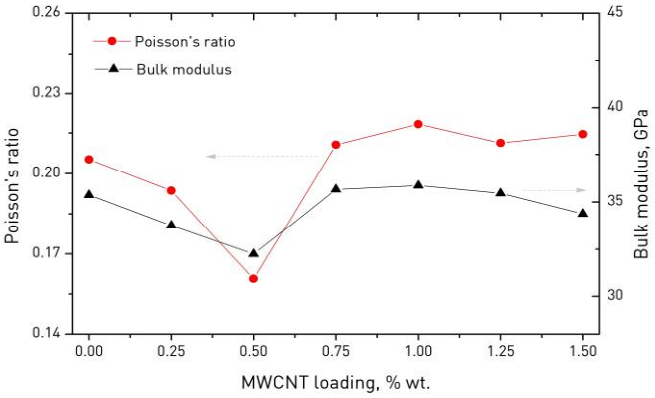

(c)

Fig. 4 Dynamic mechanical properties of MWCNT/borosilicate glass versus tube loading: Young's modulus(a), shear modulus for samples sintered at 600, 650 and 700°C (b) and Poisson's ratio (red solid cycle symbols) and bulk modulus (black solid triangle symbols) of fully dense samples sintered at 650°C (c)

Typical CNT-ceramic morphologies of fully dense CNT/ceramic samples sintered at 650°C are presented in Fig. 5. Two important overall observations were that tube integrity appeared unaffected by the high shear/high temperature sintering process and that good wetting between the tubes and the ceramic was achieved. The latter observation is particularly significant in view of the toughening potential of the tubes which requires a poreless interface with the ceramic environment to allow development of energy dissipation mechanisms [28]. Tube population density clearly increased with loading and, in many cases, large parts of the tubes lengths were exposed on the surfaces under observation, as for example in the 0.5 %wt. MWCNT-loaded ceramic depicted in Fig. 5 (a). No indications of tube dispersion inhomogeneity or agglomeration were observed for loadings below 0.75% wt. Above this concentration, pockets of entangled tubes were evident; their magnitude increased with tube concentration, as seen in Figs. 5 (b) and (c) taken from samples with CNT loadings of 1.00 and 1.50 % wt., respectively.

Indications of existence of toughening mechanisms around small microcracks and ceramic crystal boundaries were observed at almost all MWCNT loadings. Fig. 5 (d) demonstrates the failure of a single bridging nanotube in a sample with 0.50% wt. tube content; a large part of tube length is visible on the surface. While such bridging phenomena constitute a fundamental toughening/energy-dissipating mechanism for composites [29], [30], a more careful observation at the failure location reveals a very interesting effect where a number of central graphene walls remain intact to partially connect the separating tube tips. This multi-wall type of failure was very recently discovered to exhibit highly energy-dissipating potential and endow unprecedented toughening to MWCNT/alumina ceramics [26]. In fact, in a new era of CNT-reinforced matter where the effects of a thousand-fold diameter reduction are yet unclear, the specific mechanism is, along with friction due to pull-out of wavy or buckled tubes [31], [32], the only nanoscale-specific toughening mechanisms suggested to date. Indications of existence of such multiwall-type of failure in our material, coupled with findings of nanotube bridging and pull-out as seen in Figs. 5 (e) and (f), imply a high energy-dissipation potential which could be exploited for the enhancement of fracture toughness, crack growth resistance and strain tolerance of the ceramic [33]-[35]. At the same time, manufacturing of CNT-ceramics at full scales, custom geometries, low costs and high production rates can unfold advances towards complex design of high-performance components for electronic, structural, optical, biomedical and high temperature applications. To our knowledge CNTceramic manufacturing rates and dimensions similar to the ones proposed in the present methodology have not been previously reported in the literature and are a result of the uniquely efficient production route suggested herein. At the same time, final densification levels above current standards are reached due to close packing and unprecedentedly high green densities achieved by the proposed HSC technique.

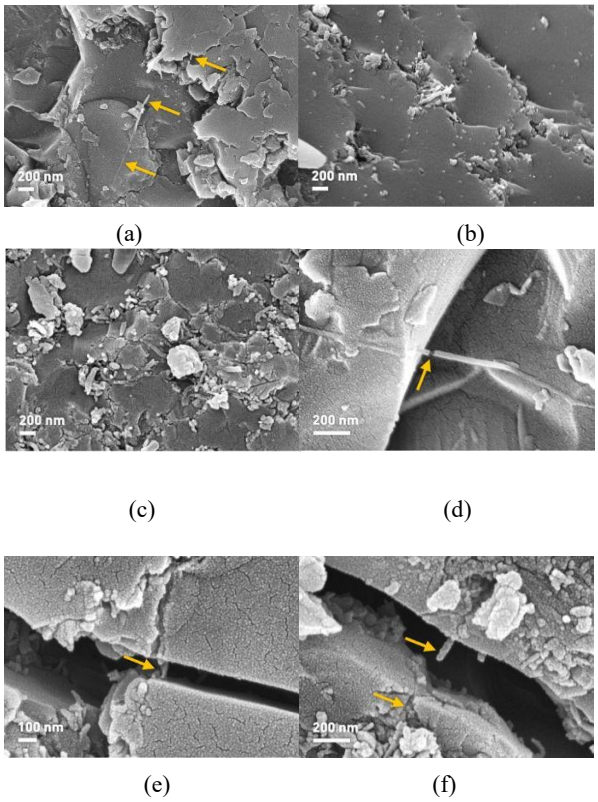

Fig. 5 SEM micrographs of surfaces of MWCNT/borosilicate glass sintered at 650°C. Unless otherwise noted, MWCNT loadings are indicated in parentheses after each caption: exposed tube surfaces and tips (0.5 %wt) (a), agglomeration pockets in a 1.00% wt. sample(b)
and worse condition in a 1.50% wt. loaded sample(c), multiwall-type nanotube failure (0.5 %wt.) (d), crack bridging by intact nanotubes (1.5%wt.) (e) and nanotube pull-out (1.5%wt.) (f). The fine craquelure pattern visible in high magnification micrographs 6.d,e and f, is artifact of the Au-sputter coating necessary for electrical conduction under SEM and is not part of material morphology

IV. Conclusion

We report a new, highly scalable and sustainable strategy which opens the doors for low cost and massive production of full scale nanotube-strenghtened ceramics. Custom forming and stacking of flexible HSC-bound green CNT-ceramic sheets of record-breaking dimensions can yield an unlimited range of three-dimensional structures while no apparent factors limit application of the technique to reinforcements, continuous media or hybrid materials different than the MWCNTs and Pyrex 7740 borosilicate glass utilized herein. The technique was systematically found associated with 100% dense final materials which dramatically improve current CNT-ceramic densification standards. MWCNT loadings of 0.5% wt. provided optimal stiffness improvement of the borosilicate glass under both shear and axial elastic loads while indications of nanoscale-specific energy dissipation mechanisms stimulate further research on the toughening and functional aspects of the novel material for a wide range of reinforcing and multifunctional applications.

REFERENCES

[1] Iijima, S., "Helical Microtubules of Graphitic Carbon," Nature, 354(6348), 56-58 (1991).
[2] Treacy, M. M. J., Ebbesen, T. W., and Gibson, J. M., "Exceptionally high Young's modulus observed for individual carbon nanotubes," Nature, 381(6584), 678-680 (1996).
[3] Yu, M. F., Lourie, O., Dyer, M. J. *et al.*, "Strength and breaking mechanism of multiwalled carbon nanotubes under tensile load," Science, 287(5453), 637-640 (2000).
[4] Balandin, A. A., "Thermal properties of graphene and nanostructured carbon materials," Nature Materials, 10(8), 569-581 (2011).
[5] Berber, S., Kwon, Y. K., and Tomanek, D., "Unusually high thermal conductivity of carbon nanotubes," Physical Review Letters, 84(20), 4613-4616 (2000).
[6] Baughman, R. H., Zakhidov, A. A., and de Heer, W. A., "Carbon nanotubes - the route toward applications," Science, 297(5582), 787-792 (2002).
[7] Berber, S., Kwon, Y. K., and Tomanek, D., "Electronic and structural properties of carbon nanohorns," Physical Review B, 62(4), R2291R2294 (2000).
[8] Avouris, P., Chen, Z. H., and Perebeinos, V., "Carbon-based electronics," Nature Nanotechnology, 2(10), 605-615 (2007).
[9] Avouris, P., Freitag, M., and Perebeinos, V., "Carbon-nanotube photonics and optoelectronics," Nature Photonics, 2(6), 341-350 (2008).
[10] Dassios, K. G., Musso, S., and Galiotis, C., "Compressive behavior of MWCNT/epoxy composite mats," Composites Science and Technology, 72(9), 1027-1033 (2012).
[11] Dassios, K., and Galiotis, C., "Polymer-nanotube interaction in MWCNT/poly(vinyl alcohol) composite mats," Carbon, (2012).
[12] Spitalsky, Z., Tasis, D., Papagelis, K. *et al.*, "Carbon nanotube-polymer composites: Chemistry, processing, mechanical and electrical properties," Progress in Polymer Science, 35(3), 357-401 (2010).
[13] Cho, J., Inam, F., Reece, M. J. *et al.*, "Carbon nanotubes: do they toughen brittle matrices?," Journal of Materials Science, 46(14), 47704779 (2011).
[14] Dassios, K. G., "Carbon nanotube-reinforced ceramic matrix composites: Processing and properties," Ceramic Transactions, 248, 133-157 (2014).
[15] Cho, J., Boccaccini, A. R., and Shaffer, M. S. P., "Ceramic matrix composites containing carbon nanotubes," Journal of Materials Science, 44(8), 1934-1951 (2009).
[16] Inam, F., Yan, H. X., Peijs, T. *et al.*, "The sintering and grain growth behaviour of ceramic-carbon nanotube nanocomposites," Composites Science and Technology, 70(6), 947-952 (2010).
[17] Peigney, A., Laurent, C., Flahaut, E. *et al.*, "Carbon nanotubes in novel ceramic matrix nanocomposites," Ceramics International, 26(6), 677683 (2000).
[18] Estili, M., and Kawasaki, A., "An approach to mass-producing individually alumina-decorated multi-walled carbon nanotubes with optimized and controlled compositions," Scripta Materialia, 58(10), 906909 (2008).
[19] Thomas, B. J. C., Shaffer, M. S. P., and Boccaccini, A. R., "Sol-gel route to carbon nanotube borosilicate glass composites," Composites Part a-Applied Science and Manufacturing, 40(6-7), 837-845 (2009).
[20] Peigney, A., Rul, S., Lefevre-Schlick, F. *et al.*, "Densification during hot-pressing of carbon nanotube-metal-magnesium aluminate spinel nanocomposites," Journal of the European Ceramic Society, 27(5), 2183-2193 (2007).
[21] Du, H. B., Li, Y. L., Zhou, F. Q. *et al.*, "One-Step Fabrication of Ceramic and Carbon Nanotube (CNT) Composites by In Situ Growth of CNTs," Journal of the American Ceramic Society, 93(5), 1290-1296 (2010).
[22] Dobedoe, R. S., West, G. D., and Lewis, M. H., "Spark plasma sintering of ceramics: understanding temperature distribution enables more realistic comparison with conventional processing," Advances in Applied Ceramics, 104(3), 110-116 (2005).
[23] Hvizdos, P., Puchy, V., Duszova, A. *et al.*, "Tribological and electrical properties of ceramic matrix composites with carbon nanotubes," Ceramics International, 38(7), 5669-5676 (2012).
[24] Tapaszto, O., Kun, P., Weber, F. *et al.*, "Silicon nitride based nanocomposites produced by two different sintering methods," Ceramics International, 37(8), 3457-3461 (2011).
[25] Zhang, S. C., Fahrenholtz, W. G., Hilmas, G. E. *et al.*, "Pressureless sintering of carbon nanotube-Al2O3 composites," Journal of the European Ceramic Society, 30(6), 1373-1380 (2010).
[26] Estili, M., Sakka, Y., and Kawasaki, A., "Unprecedented simultaneous enhancement in strain tolerance, toughness and strength of Al2O3 ceramic by multiwall-type failure of a high loading of carbon nanotubes," Nanotechnology, 24(15), (2013).
[27] Matikas, T. E., Karpur, P., and Shamasundar, S., "Measurement of the dynamic elastic moduli of porous titanium aluminide compacts," Journal of Materials Science, 32(4), 1099-1103 (1997).
[28] Estili, M., Kawasaki, A., and Sakka, Y., "Highly Concentrated 3D Macrostructure of Individual Carbon Nanotubes in a Ceramic Environment," Advanced Materials, 24(31), 4322-+ (2012).
[29] Dassios, K. G., and Galiotis, C., "Direct measurement of fiber bridging in notched glass-ceramic-matrix composites," Journal of Materials Research, 21(5), 1150-1160 (2006).
[30] Dassios, K. G., Kostopoulos, V., and Steen, M., "A micromechanical bridging law model for CFCCs," Acta Materialia, 55(1), 83-92 (2007).
[31] Xia, Z., Riester, L., Curtin, W. A. *et al.*, "Direct observation of toughening mechanisms in carbon nanotube ceramic matrix composites," Acta Materialia, 52(4), 931-944 (2004).
[32] Gu, Z. J., Yang, Y. C., Li, K. Y. *et al.*, "Aligned carbon nanotubereinforced silicon carbide composites produced by chemical vapor infiltration," Carbon, 49(7), 2475-2482 (2011).
[33] Dassios, K. G., Galiotis, C., Kostopoujos, V. *et al.*, "Direct in situ measurements of bridging stresses in CFCCs," Acta Materialia, 51(18), 5359-5373 (2003).
[34] Dassios, K. G., "A review of the pull-out mechanism in the fracture of brittle-matrix fibre-reinforced cowosites," Advanced Composites Letters, 16(1), 17-24 (2007).
[35] Dassios, K. G., Kostopoulos, V., and Steen, M., "Intrinsic parameters in the fracture of carbon/carbon composites," Composites Science and Technology, 65(6), 883-897 (2005).